

# Low-Profile Crawling for Humanoid Motion in Tight Spaces

G. Brooks, P. Krishnamurthy, and F. Khorrami

**Abstract**—While humanoid robots and various associated algorithms for gait control and motion planning have been considered in the prior literature, the possibility of utilizing a low-profile crawling gait to operate in tight spaces (e.g., going under obstacles) has not been considered previously and enables new capabilities of the humanoid robot. In this paper, a new gait for humanoid robots is presented that enables humanoid motion in tight spaces that are vertically constrained. The gait is laterally symmetric and utilizes a cooperative motion of both the hands and feet. The addition of this gait expands the set of environments that can be handled by the humanoid robot. The efficacy of the proposed gait is demonstrated experimentally on a NAO humanoid robot.

## I. INTRODUCTION

Development of a human-like robot has been a long standing objective of the robotics community. Early efforts studying legged locomotion for walking gaits and stability have been surveyed in [1], [2]. While the initial goal in study of humanoid robotic systems was for building better prosthesis and orthosis for humans (e.g., [3]), significant research effort over the past decades has addressed building of machines that are similar in shape and function to humans. Several aspects of biped humanoid robots and associated algorithms have been studied in the literature including sensing and perception, obstacle detection, navigation and path planning, gait generation, dynamic stability, and real-time control. Several small and larger size humanoids such as QRIO, NAO, PETMAN, and ASIMO, to name a few, have been developed. One of the first problems to be addressed in achieving human-like form and behavior is to mimic its mobility, i.e., walking, running, etc. Walking over uneven terrain has also been studied in [4]–[6]. Strategies for stepping over obstacles have also been addressed [7]. Biped walking over ramps has been addressed in [8] and climbing of spiral staircases has also been studied in [9]. A form of crawling based on motion on all fours (infant-like crawling) has been proposed and implemented on the NAO in [12], which represents according to [12], the first experimental implementation of a crawling gait. The all-fours infant-like crawling gait in [12] is based on the central pattern generator (CPG) from [13]. Dynamic stability of biped motion over different types of terrain/obstacles has also been addressed in [10], [11]. Navigation through an unknown environment using sensors such as vision and a laser scanner have also been addressed in many studies, e.g., [14]–[18].

To further advance the humanoid technology, DARPA has issued a grand challenge focusing on humanoids. The overall objective is a higher functionality of humanoids such as executing complex tasks in unknown, dangerous, and

The authors are with the Control/Robotics Research Laboratory (CRRL), Dept. of ECE, NYU Polytechnic School of Engineering, Brooklyn, NY 11201, USA. Corresponding author: F. Khorrami, khorrami@smart.poly.edu.

cluttered environments. For humanoid robots to be able to function in a wide range of challenging environments, a rich set of gaits and motion modalities is vital. To this end, we consider low-profile crawling motions in this paper to enable a humanoid to pass through very low openings in environments where walking or even crawling on knees (e.g., [12], [13]) would not be sufficient to clear the minimum height requirement. Unlike the infant-like all-fours crawling in [12], [13], the crawling gait proposed in this paper is designed for very low-profile motion wherein the complete body of the humanoid is essentially almost stretched out on the ground and a laterally symmetric cooperative motion of the arms and feet is used to generate forward motion (essentially a primitive pre-infant crawling/swimming motion with the whole body in close proximity to the ground). The proposed gait and its implementation have been developed and tested on the NAO robot.

This paper is organized as follows. The NAO robot platform is described in Section II. The considered gait control problem and its motivation are discussed in Section III. The details of the proposed gait and its implementation on the NAO robot are described in Section IV.



**Fig. 1:** Aldebaran Robotics NAO humanoid robot [29] at Control/Robotics Research Laboratory (CRRL).

## II. NAO HUMANOID ROBOT

NAO (Figure 1) is a humanoid experimental platform developed and commercialized by Aldebaran Robotics. The NAO at the Control/Robotics Research Laboratory (CRRL) is a 25 degree-of-freedom humanoid [30] including a number of sensors (three-axis accelerometers, two one-axis gyros, two ultrasonic sensors, four microphones, a pair of HD cameras, eight force sensors on the bottom of the feet, and two bumpers) [30]. NAO is about 58cm tall and includes a programming framework called NAOqi that provides a user friendly interface to monitor the sensors on the NAO and send control commands to achieve higher-level robot behavior. The NAOqi SDK enables the user to write custom programs for the NAO in two ways: remotely executed (from a computer that communicates with the physical NAO through a wired/wireless network) and locally executed (on

the NAO). The APIs (Application Programming Interfaces) for both modes (remote execution and local execution) follow the same structure so that code is easily portable between the two execution contexts.

The NAOqi SDK is organized into several modules that address different aspects of the NAO robot, e.g., ALMotion, ALNavigation, ALVideoDevice, ALSensors, etc. The NAO SDK also provides a set of eight pre-defined postures (within the ALRobotPosture API), including various stances, sitting, and reclining positions to any of which the robot can be commanded from any initial condition. In the context of gait control, the NAOqi SDK enables control of each joint (25 degrees of freedom in the H25 configuration) and also reading of the joint angle of each joint. Also, the current measurements for all the actuators on the robot can be accessed. While the software interface is identical in both the remote and local execution modes, the local execution mode provides a more smooth action (due to elimination of network latencies and bandwidth constraints). In particular, when logging a significant amount of data (e.g., the readings from all joint angle sensors and current sensors), the network latency limitations are more significant making the local execution mode highly preferable for efficient gaiting.

In the H25 configuration, the NAO robot includes 25 joints (which include head pitch, head yaw, etc., in addition to arm and leg joints); the primary joints of relevance for the proposed crawling gait are illustrated in Figure 2 and include: shoulder pitch ( $\theta_{sp}$ ), shoulder roll ( $\theta_{sr}$ ), elbow roll ( $\theta_{er}$ ), elbow yaw ( $\theta_{ey}$ ), hip pitch ( $\theta_{hp}$ ), hip roll ( $\theta_{hr}$ ), knee pitch ( $\theta_{kp}$ ), ankle pitch ( $\theta_{ap}$ ), and ankle roll ( $\theta_{ar}$ ).

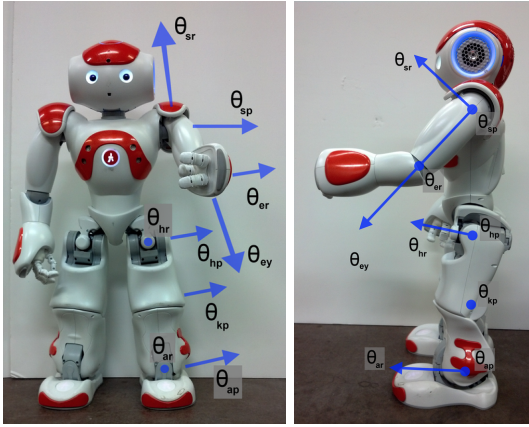


**Fig. 2: Joints of the NAO robot that are of primary relevance for the proposed crawling gait. The axes of actuation of the joints are shown as the blue vectors/dots. An axis that is normal to the plane of the figure is shown as a dot.**

### III. HUMANOID MOTION PARADIGMS

While several of the basic sub-problems of humanoid robotics are shared with other types of robots (e.g., multi-legged or wheeled robots) and unmanned vehicles, humanoid robots pose various unique aspects and sub-problems, the most significant unique aspect being, of course, the specific kinematic and dynamic motion characteristics. These motion characteristics and associated kinematic and dynamic constraints have a bearing also on more universal robotic sub-problems requiring taking these humanoid motion capabilities into account to attain a truly effective solution. For

example, while a variety of fundamental path planning and obstacle avoidance algorithms (e.g., [19]–[24]) are applicable to humanoid robots, specific algorithmic customizations and optimizations that specifically take into account the humanoid motion characteristics can provide better efficiency, robustness, and adaptability to a wide range of environments.

A motivating example for leveraging of uniquely humanoid motion capabilities for expanded robot applicability is the scenario shown in Figure 3 wherein the robot is required to perform a task (e.g., toggling a power switch or retrieving a small object) that necessitates access into a highly vertically constrained space (e.g., under a table). Performing such a task requires a very low-profile gait such as the low-profile crawling gait that is proposed in this paper (Section IV). Such a gait is relatively low-speed but due to the low profile allows access to otherwise inaccessible spaces. Typically, a humanoid application would therefore utilize a higher-speed gait such as walking for longer moves and would transition to a low-profile gait for short vertically constrained segments of the environment (e.g., Figures 7 and 8). In this context, it is interesting to note that unlike the human developmental stages of “first crawling, then walking,” a humanoid motion behavior and indeed the development of humanoid gaits rather follows the stages of “first walking, then crawling”.

### IV. HUMANOID LOW-PROFILE CRAWLING GAIT AND EXPERIMENTAL IMPLEMENTATION ON NAO ROBOT

The proposed crawling gait is illustrated in Figure 4. This gait is directly applicable to any humanoid robot which provides the basic humanoid joint structure (ankle, knee, hip, shoulder). The gait is comprised of a periodic repetition of three principal segments:

- $M_1$ : starting from a position wherein the arm and the parts of the legs below the knees (i.e., the tibia and the feet) are off the ground (the top-left picture in Figure 4, the knees are bent and the hands extended forward along the ground (to the posture shown in the top-right picture in Figure 4); this motion involves the knee pitch angles, the shoulder pitch and roll angles, and the elbow roll and yaw angles.
- $M_2$ : starting from the posture shown in the top-right picture of Figure 4), a cooperative actuation of the arm and leg joints is applied to push forward using the feet and pivot forward using the arms to the posture shown in the bottom-left picture of Figure 4. This motion involves the knee pitch angles, the ankle pitch angles, the shoulder pitch and roll angles, and the elbow roll and yaw angles, and causes the robot to translate forward with its torso raised slightly off the ground.
- $M_3$ : starting from the posture shown in the bottom-left picture of Figure 4, the robot torso is lowered down and its tibia and feet are raised back up and the arms are raised slightly to return to the initial position. This motion involves the knee pitch angles, ankle pitch angles, shoulder pitch and roll angles, and elbow yaw angles.

The bending of the knees and raising of the arms in segment  $M_3$  is performed after the chest is lowered to close to the

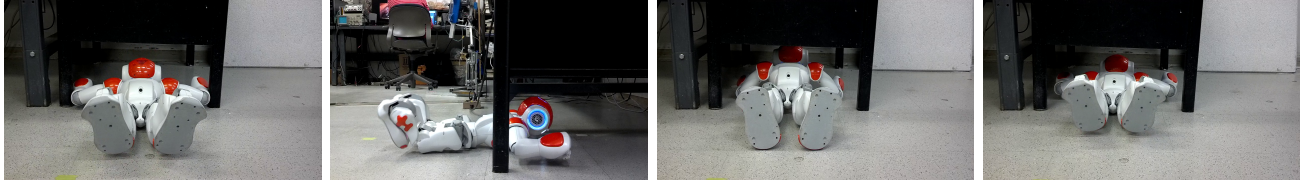


**Fig. 3:** Low-profile crawling gait for accessing vertically constrained spaces such as under a table.

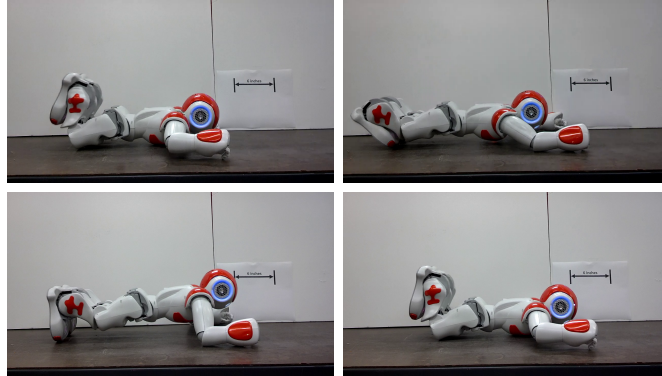


**Fig. 4:** The periodic sequence of motion segments and robot postures in the proposed low-profile crawling gait. A 6-inch marker is shown in the background as a length scale reference.

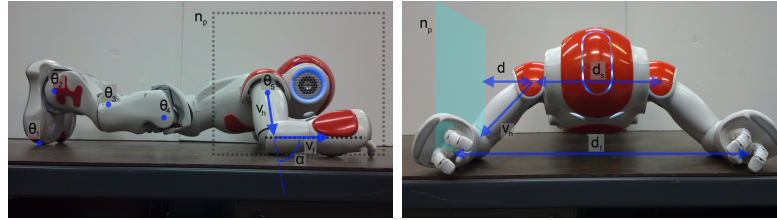


**Fig. 5:** Kinematic modeling for the motion segment  $M_2$  (the push forward) of the crawling gait.

ground. Also, the bending of the ankles in segment  $M_3$  is performed after the tibia are sufficiently off the ground so as to prevent backward motion of the robot when curling the ankles inward. This crawling gait is laterally symmetric, i.e., left-right symmetric, both in terms of the arms and legs. The cooperative motion of the arms and legs is crucial to achieve the forward crawling motion; the actuation of either just the arms or just the legs do not provide any forward motion primarily due to the motor torque constraints that do not enable overcoming of the friction for starting of forward motion with the body stretched out on the ground. The lifting of the whole body off the ground (as seen in the top-right and bottom-left figures of Figure 4) and the cooperative action of the shoulders, elbows, knees, and ankles is vital to eliminate this friction and generate efficient forward motion.

Among the motion segments  $M_1$ ,  $M_2$ , and  $M_3$ , the segment  $M_2$  is the most crucial and is the one that creates the actual forward translational motion (the push forward) and is kinematically more intricate than the other two segments. The kinematic structure of the robot during this motion segment is illustrated in Figure 5. The locations of the elbows and the tips of the feet are fixed on the ground during this motion segment (due to friction and gravity since the rest of the robot body is lifted off the ground). Thus, considering a normal plane  $n_p$  through a forearm (the right forearm for instance as shown in Figure 5) and considering the projection of the robot links on this normal plane, it is seen that an

equivalent simplified planar kinematic model of the robot can be formed for this motion segment as shown in Figure 6. In this planar kinematic model, the point at which the tips of the feet touch the ground is shown as  $(0, 0)$  and the right-most point of the “stick” model (the point at which the angle  $\alpha$  is shown) corresponds to the location at which the elbows touch the ground. The distance between these two points is fixed as described above. As the robot pushes forward during the motion segment  $M_2$ , the angle  $\alpha$  increases in magnitude (from close to around 30 degrees as shown in the top-right picture of Figure 4 to close to 90 degrees as shown in the bottom-left picture of Figure 4). The angles (with counter-clockwise angles considered to be numerically positive)  $\theta_1, \dots, \theta_5$  illustrated in Figure 6 and the left-side picture of Figure 5 correspond to the angle between the feet and the ground, the angle between the tibia and the feet, the angle between the femur and the tibia, the angle between the chest and the femur, the angle between the projection of the chest onto the normal plane  $n_p$  and the humerus (upper arm) onto the normal plane  $n_p$ , respectively. Since the robot pose is laterally symmetric as shown in Figure 5, the angles  $\theta_2$ ,  $\theta_3$ , and  $\theta_4$  correspond directly to the ankle pitch  $\theta_{ap}$ , knee pitch  $\theta_{kp}$ , and hip pitch  $\theta_{hp}$ , respectively, while the angle  $\theta_5$  corresponds to the angle between the chest and the humerus as seen in the projection on the normal plane  $n_p$ ; however, due to the kinematic construction of the NAO wherein, relative to the robot body, the shoulder pitch

is before the shoulder roll, the angle  $\theta_5$  also corresponds directly to the shoulder pitch angle  $\theta_{sp}$ . The angle  $\theta_1$  is not a controlled quantity since this is simply the angle that the feet make with the ground. Since the forearms are extended forward on the ground (as seen in Figure 5), the forearms correspond to an  $X$  axis extension to the right of the elbow point on the “stick” model in Figure 6. Hence, the angle  $\alpha$  is implicitly a function of the elbow roll and elbow yaw angles as described further below. Also, kinematically, from Figure 6, it is seen that  $\alpha = \sum_{i=1}^5 \theta_i$ .

As shown in Figure 5, the normal plane  $n_p$  is defined as the plane perpendicular to the ground and through the center line of the forearm, the forearm-to-forearm spacing is denoted by  $d_f$ , the shoulder-to-shoulder spacing is denoted by  $d_s$ . Hence, the distance from the shoulder to the plane  $n_p$  is  $d \triangleq \frac{d_f - d_s}{2}$ . Denoting the length of the humerus by  $l_h$  and the length of the humerus projected onto the plane  $n_p$  by  $\tilde{l}_h$ , we have  $\tilde{l}_h = \sqrt{l_h^2 - d^2}$ . The humerus vector (i.e., the unit vector along the center of the humerus) in three-dimensional (3D) space is given by  $v_h = [\tilde{l}_h \cos(\alpha), d, \tilde{l}_h \sin(\alpha)]^T / l_h$ . Also, the unit vector along the back of the robot written as a 3D vector is given as  $v_b = [\cos(\tilde{\theta}), 0, \sin(\tilde{\theta})]^T$  where  $\tilde{\theta} = \sum_{i=1}^4 \theta_i = \alpha - \theta_5$ . Since the forearm is oriented facing forward and placed along the ground, the unit vector along the forearm in 3D space is given by  $v_f = [1, 0, 0]^T$ . Kinematically, the combination of the elbow roll and the elbow yaw on the NAO robot can be modeled as a relation between the humerus vector and the forearm vector in the form  $R_{v_h, \theta_{ey}} R_{n_h, \theta_{er}} v_h = v_f$ . Here,  $R_{v_h, \theta_{ey}}$  denotes the rotation matrix corresponding to a rotation of angle  $\theta_{ey}$  around the vector  $v_h$  and  $R_{n_h, \theta_{er}}$  denotes the rotation matrix corresponding to a rotation of angle  $\theta_{er}$  around a vector  $n_h$  where  $n_h$  is a vector that is perpendicular to the plane passing through the center line of the humerus. Hence, the following four angles are found from the quantities described above:

- Shoulder pitch  $\theta_{sp}$  defined as the angle between the robot back and the humerus (with zero pitch defined as the humerus extended outward along the back, i.e., vertically up when the robot is in a standing position): This angle is found as the angle between the projections of  $v_h$  and  $v_b$  on the plane  $n_p$ , i.e.,  $\theta_{sp} = \cos^{-1}(\cos(\alpha) \cos(\tilde{\theta}) + \sin(\alpha) \sin(\tilde{\theta})) = \theta_5$ .
- Shoulder roll  $\theta_{sr}$ : Actuation of the shoulder roll has the effect of rotating the humerus away from the body. Hence, this angle is found from the distance  $d$  from the shoulder and the plane  $n_p$  as  $\theta_{sr} = \sin^{-1}\left(\frac{d}{\tilde{l}_h}\right)$ .
- Elbow roll  $\theta_{er}$ : The elbow roll can be found simply as the angle between the humerus vector  $v_h$  and the forearm vector  $v_f$ , i.e.,  $\theta_{er} = \cos^{-1}\left(\frac{\tilde{l}_h \cos(\alpha)}{l_h}\right)$ .
- Elbow yaw  $\theta_{ey}$ : Denoting  $\tilde{v}_h = R_{n_h, \theta_{er}} v_h$ , we get  $R_{v_h, \theta_{ey}} \tilde{v}_h = v_f$ . Hence, the unit vectors  $\tilde{v}_h$  and  $v_f$  are related by a rotation of angle  $\theta_{ey}$  around the vector  $v_h$ . Hence,  $\theta_{ey}$  can be found as  $\theta_{ey} = \cos^{-1}\left(\frac{\tilde{v}_{h,n} \cdot v_{f,n}}{\|\tilde{v}_{h,n}\| \|v_{f,n}\|}\right)$  where  $\tilde{v}_{h,n} = \tilde{v}_h - (\tilde{v}_h \cdot v_h)v_h$  and  $\tilde{v}_{f,n} = v_f - (v_f \cdot v_h)v_h$ .

For the push forward motion in segment  $M_2$ , the knee pitch and hip pitch can be nominally kept constant, i.e.,  $\theta_3$

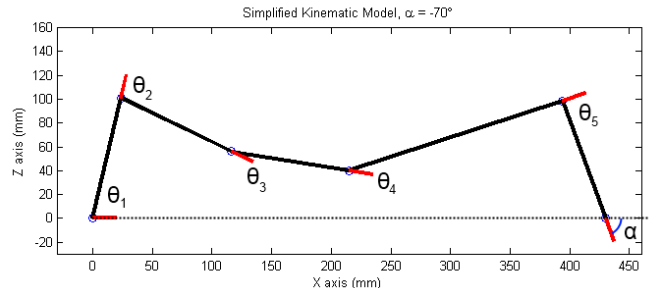


**Fig. 6: Equivalent simplified planar kinematic model (projection in the normal plane  $n_p$ ) for the motion segment  $M_2$  (the push forward) of the crawling gait.**

and  $\theta_4$  can be kept constant in the “stick” model in Figure 6. Denote the fixed distance between the tips of the feet and the elbow to be  $d_e$ . The angles  $\theta_1$ ,  $\theta_2$ , and  $\theta_5$  can be found as functions of the angle  $\alpha$  through the kinematic equations that are obtained from Figure 6 as:

$$\sum_{i=1}^5 l_i \cos(\sum_{j=1}^i \theta_j) = d_e \quad ; \quad \sum_{i=1}^5 l_i \sin(\sum_{j=1}^i \theta_j) = 0. \quad (1)$$

Using  $\sum_{i=1}^5 \theta_i = \alpha$ , equations (1) can be rewritten as

$$\sum_{i=1}^4 l_i \cos(\sum_{j=1}^i \theta_j) = d_e - l_5 \cos(\alpha) \quad (2)$$

$$\sum_{i=1}^4 l_i \sin(\sum_{j=1}^i \theta_j) = -l_5 \sin(\alpha). \quad (3)$$

If  $\theta_3$  and  $\theta_4$  are taken to be constants (or as pre-specified time trajectories), equations (2) and (3) are two equations in two unknowns  $\theta_1$  and  $\theta_2$ . Taking the square of each of the equations (2) and (3), an equation in the single variable  $\theta_2$  is obtained as:

$$2l_1 K_1 \cos(\theta_2) + 2l_1 K_2 \sin(\theta_2) = [d_e - l_5 \cos(\alpha)]^2 + [l_5 \sin(\alpha)]^2 - l_1^2 - K_1^2 - K_2^2 \quad (4)$$

where  $K_1 \triangleq l_2 + l_3 \cos(\theta_3) + l_4 \cos(\theta_3 + \theta_4)$  and  $K_2 \triangleq -l_3 \sin(\theta_3) - l_4 \sin(\theta_3 + \theta_4)$ . From this equation,  $\theta_2$  is easily solved for. In general, the equation (4) results in two possible solutions for  $\theta_2$  (the ankle pitch in this case); one of the solutions is physically not realizable since it corresponds to the ankle being turned further than its kinematic limit. Hence, the solution for  $\theta_2$  is unique. From this solution for  $\theta_2$ , the solution for  $\theta_1$  is found easily from equations (2) and (3) since with  $\theta_2$  given, these two equations correspond to two equations in the two unknowns  $\sin(\theta_1)$  and  $\cos(\theta_1)$ , thus resulting in a unique solution for  $\theta_1$ . Finally,  $\theta_5$  is found as  $\theta_5 = \alpha - \sum_{i=1}^4 \theta_i$ . Thus, the push forward motion in segment  $M_2$  of the crawling gait can be seen as a function of the single signal  $\alpha(t)$  that varies in magnitude during the push forward motion from a value  $\alpha_0$  numerically close to around -30 degrees to a value  $\alpha_1$  numerically close to around -90 degrees. As described above,  $\theta_1, \dots, \theta_5$  are obtained uniquely from  $\alpha$  after which the elbow roll and yaw and the shoulder pitch and roll are obtained as also described above. Finally, these angles are mapped to the physical robot joint angles accounting for offsets in the definitions of the angles

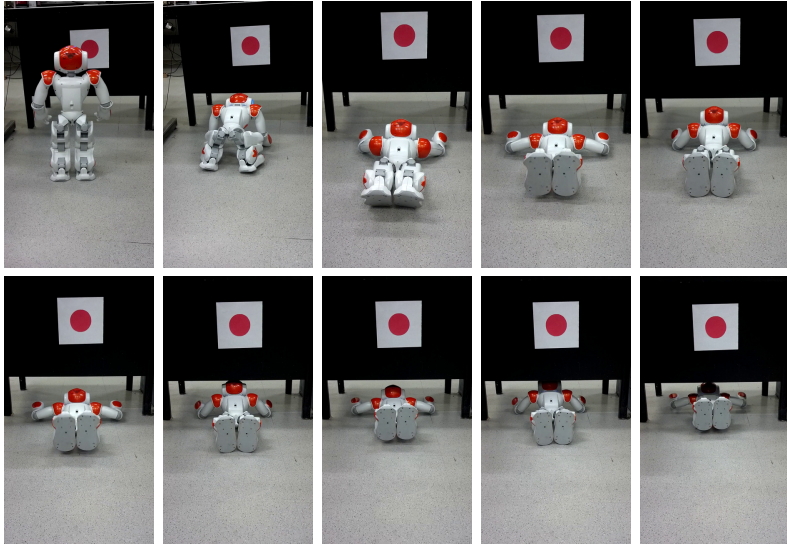


**Fig. 7:** Approaching and crawling under an obstacle. A red dot is used as a marker for the direction in which the robot is commanded to move. When the robot approaches below a specified distance threshold from the obstacle, the crouch-down and crawl gait sequence is initiated.

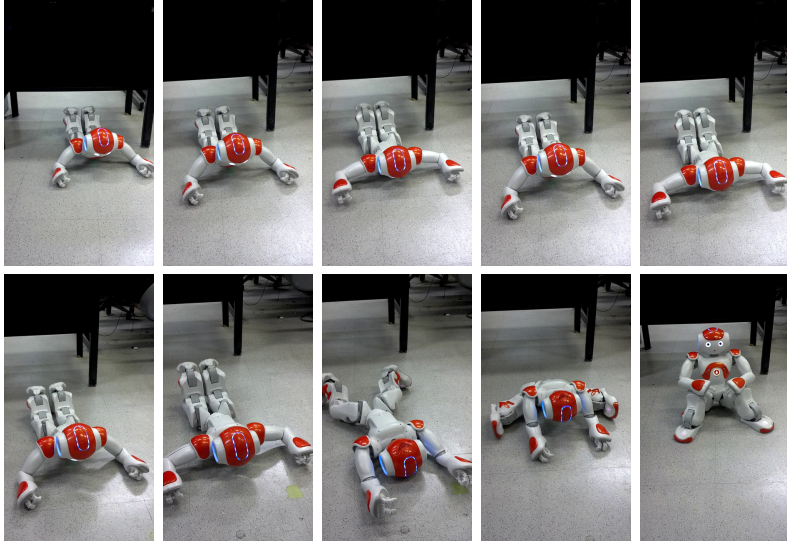


**Fig. 8:** Crawling under an obstacle and transitioning back to stand posture.

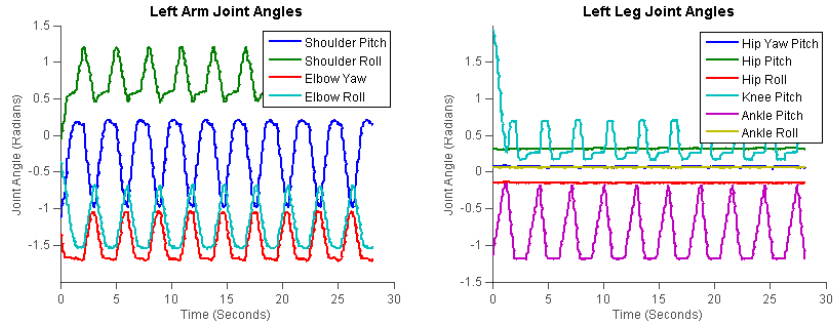


**Fig. 9:** Measured motor joint angles during multiple iterations of the periodic crawling gait. While the crawling gait is laterally symmetric, the asymmetry in measured angles is due to the definitions of the robot frame and joint frame in the NAO API, which essentially forms a mirror asymmetry between the left and right joints.

[30] and the mirror symmetries between the angle definitions on the left and right sides of the robot.

The initial and final configurations during the push forward motion are specified by initial and final values of  $\alpha$ ,  $\theta_3$ , and

$\theta_4$ ; as described above, the other joint angles (ankle pitch  $\theta_2$ , shoulder pitch  $\theta_5$ , and the angle  $\theta_1$ ) can be found from this angle triplet. The knee pitch  $\theta_3$  and hip pitch  $\theta_4$  can be taken to be nominally constants and hence have the same initial

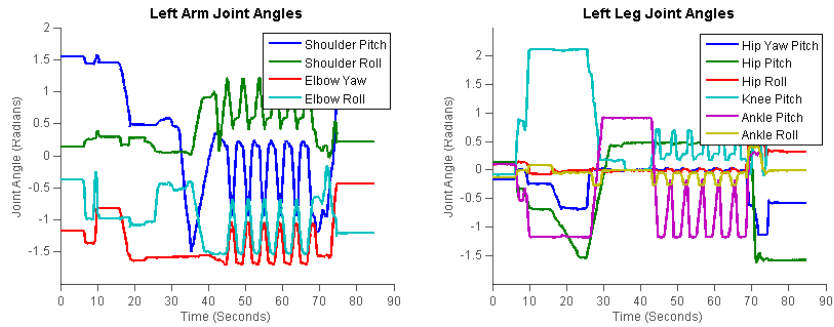


**Fig. 10: Measured joint angles for a sequence of transitioning from standing to crouch to crawling, crawling under a table, and then returning to crouch.**

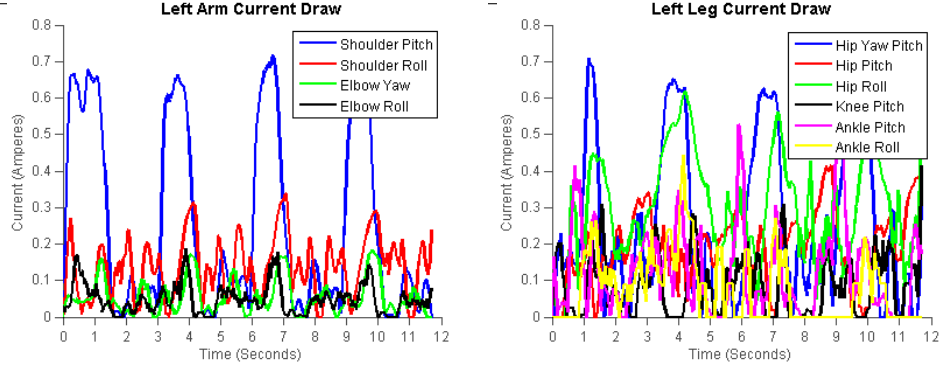


**Fig. 11: Measured motor current draws during multiple iterations of the periodic crawling gait.**

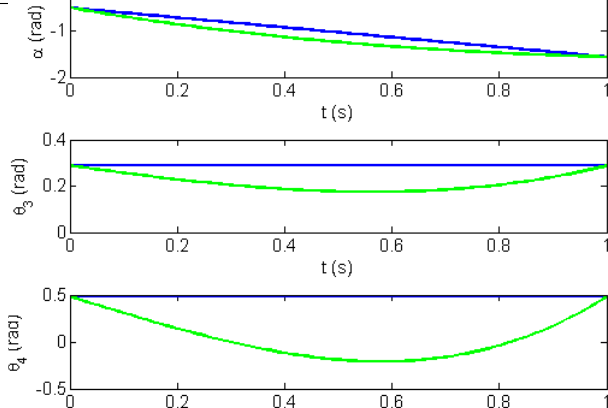


**Fig. 12: Optimization of crawling motion. Blue lines: nominal time trajectories of the angle triplet  $(\alpha, \theta_3, \theta_4)$ ; Green lines: optimized time trajectories.**

and final values. The angle  $\alpha$  varies from an initial to a final value. The simplest time interpolation of this “free” angle triplet  $(\alpha, \theta_3, \theta_4)$  is a straight line interpolation keeping  $\theta_3$  and  $\theta_4$  constant and varying  $\alpha$  monotonically. However, the degrees of freedom in specifying the time trajectory of this angle triplet subject to initial and final value constraints can be utilized to satisfy auxiliary requirements or to optimize some aspects of the crawling motion. For example, one immediate application of this freedom in specifying the angle triplet time trajectory is to optimize torque requirements during the crawling motion. For simplicity, since the crawling motion is a relatively slow dynamic motion, a pseudo-static approximation of the relevant torques ( $\tau_1$ ,  $\tau_2$ ,  $\tau_3$ , and  $\tau_4$  being the ankle pitch torque, knee pitch torque, hip pitch torque, and shoulder pitch torque, respectively, with each of these torques taken as averages of the right-side and left-side

joints) can be used. Since torque sensors are not directly available on the NAO robot, a simulated NAO dynamic model in the v-rep simulation platform [31] was utilized to generate a look-up table of torque values (for each of  $\tau_1$ ,  $\tau_2$ ,  $\tau_3$ , and  $\tau_4$ ) as functions of  $(\alpha, \theta_3, \theta_4)$ . Based on this look-up table, an optimization of the time trajectories for  $(\alpha(t), \theta_3(t), \theta_4(t))$  over the time interval  $t \in [0, T]$  subject to initial and final value constraints is shown in Figure 12; the optimization cost here is defined as  $\int_0^T \sum_{i=1}^4 w_i \tau_i^2(t) dt$  with the integral evaluated as a finite sum approximation, where  $T$  is the time interval (e.g.,  $T = 1$  s) for the push forward motion.  $w_i, i = 1, \dots, 4$ , are weights specified here to be 1, 1, 1, and 5, respectively (the higher weight on the shoulder pitch models the fact that the shoulder pitch joint motor is a weaker motor on the NAO). In addition,  $\alpha$  is constrained to be monotonic decreasing to prevent backtracking and the joint limits of the physical robot are included in the optimization cost. The time trajectories for  $(\alpha(t), \theta_3(t), \theta_4(t))$  are parameterized as separate cubic splines and a simple genetic algorithm (implemented in Matlab) is utilized to optimize the parameters of the cubic splines. The optimized time trajectories (green lines in Figure 12) correspond to the value 0.68 for the optimization cost defined above while the nominal time trajectories correspond to the value 1.85 for the optimization cost.

Another application of this freedom in specifying the angle triplet time trajectory is to command the orientation of the robot back. With control of this parameter, the robot could, for example, orient a back mounted laser scanner, augment neck orientation for better visibility from the NAO’s head mounted cameras, or shift the NAO’s center of mass (CoM) during gaiting. This can be particularly beneficial when crawling over inclines or declines where shifting the

CoM can help preserve gait stability by redistributing the application of force to the ground. Also, note that by utilizing different parameters for the time trajectories on the right-side and left-side joints, differential crawling can also be achieved to adapt the crawling direction.

Also, the proposed gait is scalable to different relative sizes and joint configurations of the humanoid robot. As the core motion is parameterized through the “stick” model via the angle  $\alpha$ , producing the actuated angles  $\theta_2$  and  $\theta_5$ , any robot whose profile projected onto the sagittal plane can produce a parallelogram structure can utilize the proposed gait. Portions of the angles  $\theta_2$  and  $\theta_5$  can be redistributed to other joint angles, such as  $\theta_3$  and  $\theta_4$ , in order to achieve the  $\alpha$  angle. For example, a limbed robot with four degrees of freedom per limb could distribute the value of  $\theta_2$  to its rear limb joints and distribute  $\theta_5$  to its forward limb joints and produce the gaiting motion. In contrast, a robot with only one degree of freedom per limb can also produce this gait, as effectively demonstrated by the NAO. Due to its simple structure, the proposed low-profile crawling gait is applicable to a wide range of humanoid platforms.

The sequence of the motion segments  $M_1$ ,  $M_2$ , and  $M_3$  described above can be performed at different numbers of sequences per second to generate different speeds. Typically, sequence repetition rates of one sequence every 1.5 to 2 seconds (or more for slower crawling) can be utilized for continuous crawling at forward translational speeds around 1 ft per 6 to 8 seconds. The highest point on the robot during this crawling gait is the top of the head which at the highest point in the sequence is around 8 inches off the ground providing a low-profile gait that enables crawling through highly vertically constrained spaces (e.g., Figures 7 and 8). In comparison, a walking gait requires a vertical clearance of at least 23 inches and an infant-like all-fours crawling requires well over a foot of vertical clearance.

Sample experimental runs of the proposed crawling gait on the NAO robot are shown in Figures 3, 4, 7, and 8. A complete sequence of transitioning from walking to a crouch posture and then crawling under a table and finally getting back to crouch and stand postures is shown in Figures 7 and 8. For transitioning from stand to crouch, the built-in crouch posture in the ALRobotPosture API of the NAO SDK is used. From the crouching posture, in which the robot is on its feet, with the femur resting on the tibia and the torso held upright, a sequence of joint motions is applied to transition to the initial position of the crawl gait (top-left picture of Figure 4). The joint angles and the motor current draws measured during experimental runs on the NAO are also shown in Figures 9, 10, and 11.

## V. CONCLUSION

In this paper, a new gait for humanoid robots was presented to enable low-profile crawling. The proposed gait is particularly useful when the humanoid robot is required to operate in tight vertically constrained spaces (*crawl* spaces) such as when the robot needs to move under an obstacle that partially blocks the robot path but has a small clearing underneath that can be moved through with a sufficiently low profile gait. The proposed gait is laterally symmetric

and utilizes a cooperative motion of both the hands and feet. The efficacy of the proposed gait was demonstrated experimentally on a NAO humanoid robot. In currently ongoing work, the characteristics of the proposed low-profile crawling gait are being further studied and optimized for forward translational speed and power efficiency and motor joint stresses. Also, a multi-motion-mode framework for humanoid motion planning is being developed that leverages the walking and crawling capabilities for agile navigation through challenging environments including transitions between walking and crawling depending on the local obstacle geometry and commanded tasks.

## REFERENCES

- [1] M. Vukobratović and B. Borovac, “Zero-moment point thirty five years of its life,” *International Journal of Humanoid Robotics*, vol. 1, no. 1, pp. 157173, 2004.
- [2] P. Holmes, R. J. Full, D. Koditschek, and J. Guckenheimer, “The dynamics of legged locomotion: models, analyses, and challenges,” *SIAM Review*, vol. 48,no. 2, pp. 207304, 2006.
- [3] D. E. Whitney, “Resolved motion rate control of manipulators and human prostheses,” *IEEE Transactions on Man-Machine Systems*, vol. 10, no. 2, pp. 47–53, June 1969.
- [4] F. Iida and R. Tedrake, “Minimalistic control of biped walking in rough terrain,” *Autonomous Robots*, pp. 355-368, April 2010.
- [5] J.-c. Wu and Z. Popović, “Terrain-adaptive bipedal locomotion control,” *ACM Trans. on Graphics*, vol. 29, no. 4, July 2010.
- [6] J. Chestnutt, J. Kuffner, K. Nishiwaki, and S. Kagami, “Planning biped navigation strategies in complex environments,” in *Proc. of the 2003 IEEE International Conf. on Humanoid Robotics*, (Karlsruhe, Germany), Sept. 2003.
- [7] B. Verrelst, O. Stasse, K. Yokoi, B. Vanderborght, “Dynamically stepping over obstacles by the humanoid robot HRP-2,” in *Proc. of the IEEE-RAS International Conf. on Humanoid Robots*, (Genova, Italy), Dec. 2006.
- [8] C. Lutz, F. Atmanspacher, A. Hornung, and M. Bennewitz, “NAO walking down a ramp autonomously,” in *Proc. of the IEEE/RSJ International Conf. on Intelligent Robots and Systems*, (Vilamoura, Portugal), Oct. 2012.
- [9] S. Oswald, A. Gorog, A. Hornung, and M. Bennewitz, “Autonomous climbing of spiral staircases with humanoids,” in *Proc. of the IEEE/RSJ International Conf. on Intelligent Robots and Systems*, (San Francisco, CA), Sept. 2011.
- [10] E.R. Westervelt, J.W. Grizzle, C. Chevallereau, J.H. Choi, and B. Morris. Feedback control of dynamic bipedal robot locomotion. *CRC Press*, 2007.
- [11] C. Chevallereau, D. Djoudi, and J.W. Grizzle, “Stable bipedal walking with foot rotation through direct regulation of the zero moment point”, *IEEE Trans. on Robotics*, vol. 25, no. 2, pp. 390-401, April 2008.
- [12] C. Li, R. Lowe, B. Duran, and T. Ziemke, “Humanoids that crawl: Comparing gait performance of iCub and NAO using a CPG architecture,” in *Proc. of the IEEE International Conference on Computer Science and Automation Engineering*, (Shanghai, China), June 2011.
- [13] L. Righetti and A. Jan Ijspeert, “Design methodologies for central pattern generators: an application to crawling humanoids,” in *Proc. of Robotics: Science and Systems*, (Philadelphia, PA), pp. 191198, 2006.
- [14] J. Chestnutt, Y. Takaoka, K. Suga, K. Nishiwaki, J. Kuffner, and S. Kagami, “Biped navigation in rough environments using on-board sensing,” in *Proc. of the IEEE/RSJ International Conf. on Intelligent Robots and Systems*, (St. Louis, MO), Oct. 2009.
- [15] A. Yamashita, M. Kitaoka, and T. Kaneko, “Motion planning of biped robot equipped with stereo camera using grid map,” *International Jour. of Automation Technology*, vol. 5, no. 5, pp. 639-647, 2011.
- [16] P. Michel, J. Chestnutt, S. Kagami, K. Nishiwaki, J. Kuffner, and T. Kanade, “Online environment reconstruction for biped navigation,” in *Proc. of the IEEE International Conf. on Robotics and Automation*, (Orlando, Florida), May 2006.
- [17] R. Ozawa, Y. Takaoka, Y. Kida, K. Nishiwaki, J. Chestnutt, J. Kuffner, S. Kagami, H. Mizoguchi, and H. Inoue, “Using visual odometry to create 3D maps for online footstep planning,” in *Proc. of the IEEE International Conf. on Systems, Man and Cybernetics*, (Big Island, HI), Oct. 2005.
- [18] J.-S. Gutmann, M. Fukuchi, and M. Fujita, “3D Perception and Environment Map Generation for Humanoid Robot Navigation,” *International Journal of Robotics Research*, vol. 27, no. 10, pp. 1117-1134, Oct. 2008.
- [19] J. C. Latombe, *Robot Motion Planning*. Norwell, MA: Kluwer Academic Publishers, 1991.
- [20] S. Russell and P. Norvig, *Artificial Intelligence: A Modern Approach*. Saddle River, NJ: Prentice Hall, 2009.

- [21] O. Khatib, "Real-time obstacle avoidance for manipulators and mobile robots," in *Proc. of the IEEE International Conf. on Robotics and Automation*, March 1985, pp. 500–505.
- [22] E. Rimon and D. E. Koditschek, "Exact robot navigation using artificial potential functions," *IEEE Trans. on Robotics and Automation*, vol. 8, no. 5, pp. 501–518, Oct. 1992.
- [23] A. Stentz, "Optimal and efficient path planning for partially-known environments," in *Proc. of the IEEE International Conf. on Robotics and Automation*, San Diego, CA, May 1994, pp. 3310–3317.
- [24] P. Krishnamurthy and F. Khorrami, "GODZILA: A low-resource algorithm for path planning in unknown environments," *Jour. of Intelligent and Robotic Systems*, vol. 48, no. 3, pp. 357–373, March 2007.
- [25] P. Krishnamurthy, F. Khorrami, and T. L. Ng, "Obstacle avoidance for unmanned sea surface vehicles: a hierarchical approach," in *Proc. of the 2008 IFAC World Congress*, Seoul, Korea, July 2008.
- [26] F. Khorrami and P. Krishnamurthy, "A hierarchical path planning and obstacle avoidance system for an autonomous underwater vehicle," in *Proc. of the American Control Conf.*, (St. Louis, MO), June 2009.
- [27] P. Krishnamurthy and F. Khorrami, "A hierarchical control and obstacle avoidance system for Unmanned Sea Surface Vehicles," in *Proc. of the IEEE Conf. on Decision and Control/ European Control Conf.*, (Orlando, FL), pp. 2070–2075, Dec. 2011.
- [28] G. Brooks, P. Krishnamurthy, and F. Khorrami, "Humanoid robot navigation and obstacle avoidance in unknown environments," in *Proc. of the Asian Control Conference*, (Istanbul, Turkey), June 2013.
- [29] NAO Humanoid Robot. <http://www.aldebaran-robotics.com>.
- [30] Components of NAO Humanoid Robot. [http://www.aldebaran-robotics.com/documentation/family/nao\\_h25/index\\_h25.html](http://www.aldebaran-robotics.com/documentation/family/nao_h25/index_h25.html).
- [31] v-rep: virtual robot experimentation platform. <http://www.coppeliarobotics.com>.